Available online at www.sciencedirect.com

jmr&t Journal of Materials Research and Technology

journal homepage: www.elsevier.com/locate/jmrt

Original Article

Electrical and dielectric properties of rare earth substituted hard-soft ferrite $(Co_{0.5}Ni_{0.5}Ga_{0.01}Gd_{0.01}Fe_{1.98}O_4)_x/(ZnFe_2O_4)_y$ nanocomposites

M.A. Almessiere [a,b,*], B. Unal [c], A. Demir Korkmaz [d], Sagar E. Shirsath [e], A. Baykal [f], Y. Slimani [b], M.A. Gondal [g,h], U. Baig [i], A.V. Trukhanov [j,k,l]

[a] Department of Physics, College of Science, Imam Abdulrahman Bin Faisal University, P.O. Box 1982, Dammam 31441, Saudi Arabia

[b] Department of Biophysics, Institute for Research and Medical Consultation (IRMC), Imam Abdulrahman Bin Faisal University, P.O. Box 1982, Dammam 31441, Saudi Arabia

[c] Institute of Forensic Sciences and Legal Medicine, Istanbul University-Cerrahpasa, Buyukcekmece Campus, 34500 Buyukcekmece, Istanbul, Turkey

[d] Department of Chemistry, Istanbul Medeniyet University, 34700 Uskudar, Istanbul, Turkey

[e] School of Materials Science and Engineering, University of New South Wales, Kensington, NSW 2052, Sydney, Australia

[f] Department of Nanomedicine Research, Institute for Research and Medical Consultation (IRMC), Imam Abdulrahman Bin Faisal University, P.O. Box 1982, Dammam 31441, Saudi Arabia

[g] Laser Research Group, Physics Department & IRC-Hydrogen and Energy Storage, King Fahd University of Petroleum and Minerals, 31261, Dhahran, Saudi Arabia

[h] K.A.CARE Energy Research and Innovation Center, King Fahd University of Petroleum and Minerals, 31261, Dhahran, Saudi Arabia

[i] Interdisciplinary Research Center for Membranes and Water Security, King Fahd University of Petroleum and Minerals, 31261, Dhahran, Saudi Arabia

[j] South Ural State University, 454080, Chelyabinsk, Russia

[k] SSPA "Scientific and Practical Materials Research Centre of NAS of Belarus", 220072, Minsk, Belarus

[l] L.N. Gumilyov Eurasian National University, 010000, Nur-Sultan, Kazakhstan

ARTICLE INFO

Article history:
Received 18 July 2021
Accepted 13 August 2021
Available online 20 August 2021

Keywords:
Hard-soft spinel ferrite
nanocomposite

ABSTRACT

$ZnFe_2O_4$ (ZFO) NPs (nanoparticles), $Co_{0.5}Ni_{0.5}Ga_{0.01}Gd_{0.01}Fe_{1.98}O_4$ (CNGaGdFO) NPs and hard-soft spinel ferrite (H/S) $(CNGaGdFO)_x/(ZFO)_y$ (x:y = 1:1, 1:2, 1:3, 2:1, 3:1 and 4:1) NCs (nanocomposites) were synthesized via a one-pot sol–gel auto combustion route. X-ray powder diffraction (XRD) analyses confirmed the purity of ZFO NPs, CNGaGdFO NPs and H/S (H/S) $(CNGaGdFO)_x/(ZFO)_y$ (x:y = 1:1, 1:2, 1:3, 2:1, 3:1 and 4:1) (absence of any second phase). The crystallite size of NCs was between 39 and 52 nm. The cubic morphology was observed for ZFO NPs, CNGaGdFO NPs and all H/S NCs by the help of scanning electron microscopy (SEM) and transmission electron microscopy (TEM) analyses. Energy dispersive

* Corresponding author.
E-mail address: malmessiere@iau.edu.sa (M.A. Almessiere).

https://doi.org/10.1016/j.jmrt.2021.08.049

Conductivity
Electrical and dielectric properties
Diffuse reflectance
$CoFe_2O_4$
$ZnFe_2O_4$

X-Ray analysis (EDX) also confirmed the chemical formula of all the NC samples. Electrical and dielectric properties of ZFO NPs, CNGaGdFO NPs and H/S NCs were explored with an impedance analyzer with f ≤ 3.0 MHz, where f stands for frequency, and within the temperature range between 20 and 120 °C. Electric and dielectric parameters such as AC conductivity as well as DC conductivity, activation energy, dielectric constant, dielectric loss in addition to the dissipation parameter relevant to the electrical energy due to different physical processes were measured for each of the given compositional ratios. The AC conductivity was found to follow the frequency-dependent power law in general, being mainly reliant on the compositional ratios and the measured temperatures especially at lower frequencies. This study has shown that CoNiGaGdFeO-$ZnFe_2O_4$ H/S NCs carry out conduction mechanisms, which can be predominantly credited to grain–grain boundaries for various compositional ratios. The dielectric constant of $(CNGaGdFO)_x/(ZFO)_y$ (x:y = 1:1, 1:2, 1:3, 2:1, 3:1 and 4:1) H/S NCs indicates common dielectric behaviours with frequency, largely dependent on compositional rates of the hard to soft spinel ferrites. It is observed that hard ferrite is dominant in the formation of the semicircles, and the diameter of the semicircles shows a drop as the temperature rises, suggesting a temperature-dependent relaxation mechanism. Consequently, the observed variation of the studied dielectric parameters with frequency can be explained by the conduction mechanism in most composition ratios of hard to soft spinel ferrites, which can be explained by a phenomenological method with Koop's model.

1. Introduction

Due to their technological importance, nanospinel ferrites have wide applications from biomedical to industrial sectors, such as cancer diagnosis, drug delivery, cancer gene therapy, as catalyst, in high-frequency device, gas sensor, etc. [1]. Spinel ferrites are soft ferrites (MFe_2O_4, M^{2+} represents the metal ions) having moderate Ms (saturation magnetization), low anisotropy, low coercivity (Hc), high initial permeability and low eddy current loss [2,3]. In normal spinel ferrites, M(T_d-site) Fe_2(O_h-site) O_4, ferric ions exist in O_h sites while M^{2+} ions are in T_d sites (O_h: octahedral and T_d: tetrahedral). $ZnFe_2O_4$ has normal spinel ferrite structure. In inverse spinel ferrites, ($[M^{2+}\ Fe^{3+}]^B\ [Fe^{3+}]^A\ O_4$), ½ of the iron (III) ions occupy T_d-sites and the rest of ions reside in O_h-sites ($NiFe_2O_4$, $CoFe_2O_4$, etc.).

Thanks to its high magnetic moment, moderate Ms (saturation magnetization), high anisotropy, good chemical and physical stability, $CoFe_2O_4$ (CFO) can be considered as a hard magnet [4]. Hence, $CoFe_2O_4$ NPs find applications in magnetic recording technology, including but not limited to high-density digital recording disks, audiotapes, videotapes, etc. [5]. On the other hand, the smaller toxicity of zinc (II) led $ZnFe_2O_4$ (ZFO) NPs to be utilized in nanomedicine, such as MRI contrast agents [6]. The atomic sizes and crystal structures of ZFO and CFO are similar and hence novel NCs containing both compounds and their compositions can be fabricated and evaluated for their electrical and dielectric properties. In addition, more novel properties can be obtained when rare elements are incorporated in their structure.

The substitution of rare earths into the spinel structure leads to a distortion in the structure and introduces strains, thus altering the magnetic and electrical behavior significantly [7]. The control of rare earth and/or metal ion substituents of various types also results in altering electromagnetic properties of NCs by controlling different types and amounts of metal ion or substitution [8–10].

Recently, ferrite nanocomposites have been the subject of much research because of their extensive technological and industrial applications. These nanocomposites are built from two magnetic phases which are also known as bi-magnetic composites. The presence of strong coupling among distinctive constituents in NCs gives rise to unique physical characteristics as well as superior properties, making these nanocomposites exceptional compared to their individual components counterparts for biomedicine, spintronics, optoelectronics and nanoelectronics applications [11]. Accordingly, a various of researchers have been reported a unique physical feature of these type of nano-compositions. S.F. Mansour et al. Synthesized nanocomposites consisted of different factions of ((1-y) $Bi_{0.8}La_{0.2}Fe_{0.92}Cr_{0.08}O_3$+(y) $CoFe_2O_4$ (y = 0.0. 0.5, 0.6, 0.7, 0.8, and 1.0) [12]. They found that the magnetic and dielectric properties were introduced an improvement compared with separate phase of the composite. F. Hosseini Mohammadabadi et al. studied the Electromagnetic microwave absorption properties of $((MnNiCuZn)_{1-x}Co_xFe_2O_4)$/graphene nanocomposites (x = 0.05, 0.1, 0.2, and 0.3) [13]. They observed the coercivity increased with changing the Co ratios, while the saturation magnetization slightly changed. Furthermore, Chao Feng et al. investigated the microwave absorption of Core/shell hard/soft spinel-ferrite-based $CoFe_2O_4/NiFe_2O_4$ [4]. They noticed that the core/shell structure has a significant decrease in electric resistivity and an improvement in dipole and interfacial polarizations in the

CFO/NFO, subsequent a clear increase in dielectric permittivity and loss in the whole S–Ku bands.

Consequently, to the extent of our knowledge, this is the first paper reporting the synthesis of hard/soft spinel ferrites with x and y ratios, $(CNGaGdFO)_x/(ZFO)_y$ (x:y = 1:1, 1:2, 1:3, 2:1, 3:1 and 4:1), NCs by cost-effective method of sol– gel coupled with a self-combustion process which requires a minimal effort.

2. Experimental

2.1. Chemicals and instrumentations

All metal nitrates ($Zn(NO_3)_2$, $Fe(NO_3)_3.9H_2O$, $Ni(NO_3)_2$, $Ga(NO_3)_3$, $Gd(NO_3)_3$, NH_3 solution and citric acid with high purity were obtained from Merck. A D/MAX-2400 (Cu Kα) X-ray powder diffractometer (Rigaku, Japan) was used to study the crystal phases of soft and hard ferrites. SEM, TEM and high resolution TEM (HR-TEM) (FEI Titan ST Microscopes) were employed for morphological analyses. Dielectric parameters were verified with the help of an Alpha-N impedance analyzer with high-resolution (Novocontrol, Germany).

2.2. Synthesis

A sol–gel auto-combustion was employed to prepare the ZFO NPs, CNGaGdFO NPs individually and hard/soft spinel ferrite H/S $(CNGaGdFO)_x/(ZFO)_y$ (x:y = 1:1, 1:2, 1:3, 2:1, 3:1 and 4:1) NCs.

Part A: ZFO NPs was prepared using sol–gel auto combustion by mixing $Fe(NO_3)_39H_2O$, $Zn(NO_3)_2$ and citric acid in 80 mL of deionized water with continuous stirring for 30 min 80 °C. An ammonia solution was applied to the reaction mixture for reaching neutral pH followed by increasing the temperature to 160 °C for 50 min and lastly to 380 °C to obtain powder of black color. The final product was obtained by calcining at 700 °C for 4 h.

Part B: CNGaGdFO NPs were obtained by applying the similar procedure in *Part A*. $Co(NO_3)_2$, $Ni(NO_3)_2$, $Ga(NO_3)_3$,-$Gd(NO_3)_3$ and $Fe(NO_3)_39H_2O$ along with $C_6H_8O_7$ were stirred in 80 mL of DI H_2O. The pH was adjusted at 7 by ammonia solution, and the temperatures were raised to 160 °C for 50 min and 380 °C until the whole solution turn to gel then burn yielding a black powder, which was then calcined at 700 °C for 4 h.

Part C: The fractions of H/S $(CNGaGdFO)_x/(ZFO)_y$ (x:y = 1:1, 1:2, 1:3, 2:1, 3:1 and 4:1) NCs were prepared by One-pot sol–gel auto-combustion method. Firstly, A solutions of ZFO by mixing $Fe(NO_3)_39H_2O$ and $Zn(NO_3)_2$ in 50 mL of deionized water and a solution of CNGaGdFO by mingling $Co(NO_3)_2$, $Ni(NO_3)_2$, $Ga(NO_3)_3$,$Gd(NO_3)_3$ and $Fe(NO_3)_39H_2O$ with 50 mL of deionized water. After that, both ZFO and CNGaGdFO solutions were mixed and added $C_6H_8O_7$. After. pH = 7 was regulated by NH_3 solution, the reaction mixture was stirred firstly at 160 °C for 50 min and then at 380 °C. The samples, which were composed of black powders, were heated in muffle furnace at 950 °C for 4 h.

3. Results and discussion

3.1. Crystal phase evaluation

Phase analyses of ZFO NPs, CNGaGdFO NPs and H/S $(CNGaGdFO)_x/(ZFO)_y$ (x:y = 1:1, 1:2, 1:3, 2:1, 3:1 and 4:1) NCs were proceeded through XRD and diffractograms can be seen in Fig. 1. Every composition displayed pure cubic spinel ferrite phase typical peaks with no occurrence of any undesirable phase. Obviously, there appears to be a slight change in the intensity of the characteristic peaks of the spinel structure with altering the CNGaGdFO and ZFO NPs because of crystallization. Table 1 shows the structure parameters, crystallite size and cell volume for all hard/soft NCs compositions of were estimated by Match 3! software. The structural parameter "a_o" H/S NCs varies with changing the fraction between CNGaGdFO and ZFO NPs. Match 3! software was employed to calculate the crystallite size via Scherrer's equation and existed in the range of 38–59 nm.

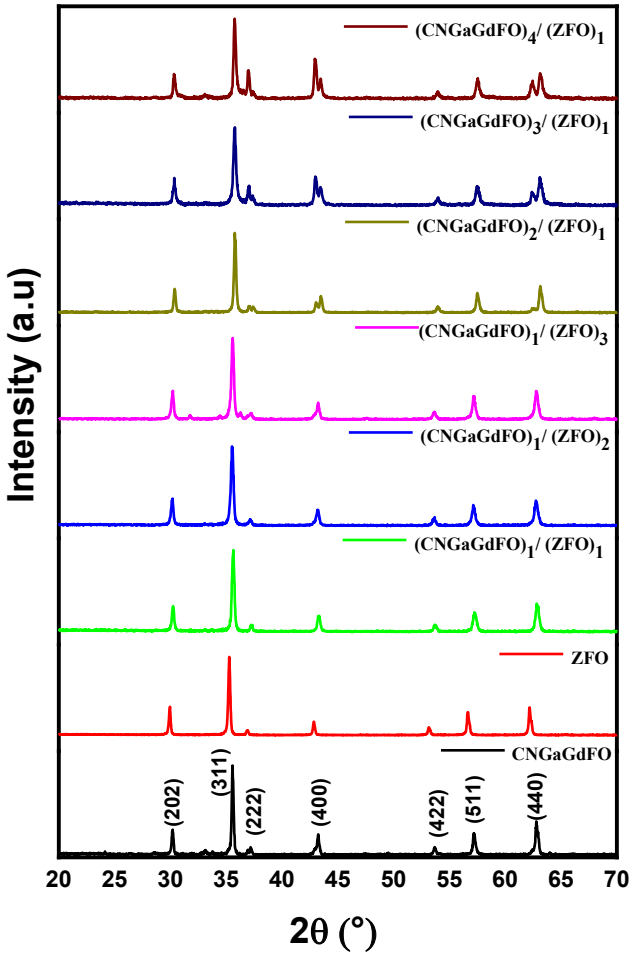

Fig. 1 – XRD powder patterns of CNGaGdFO NPs, ZFO NPs and H/S $(CNGaGdFO)_x/(ZFO)_y$ (x:y = 1:1, 1:2, 1:3, 2:1, 3:1 and 4:1) NCs.

3.1.1. Cation distribution

Cation distribution estimation of H/S $(CNGaGdFO)_x/(ZFO)_y$ (x:y = 1:1, 1:2, 1:3, 2:1, 3:1 and 4:1) NCs has been carried out by Bersatu's method [14]. The cation distribution was estimated by X-ray diffraction intensities of (220), (440), (422) and (400) planes which are sensitive to cation distribution [15]. XRD patterns indicate the presence of three phases in the compositions, such as CNGaGdFO NPs, ZFO NPs and H/S $(CNGaGdFO)_x/(ZFO)_y$ NCs. In case of pure phase of H/S $(CNGaGdFO)_x/(ZFO)_y$ (x:y = 1:1, 1:2, 1:3, 2:1, 3:1 and 4:1) NCs, Ga^{3+} and Gd^{3+} ions with larger ionic radii reside in O_h B-site. 80% of Ni^{2+} and Co^{2+} ions prefer to occupy the O_h-B site, whereas 20% of them occupy the T_d A-site. Inverse spinel structure containing nickel (II) and cobalt (II) ions are supposed to occupy O_h B-site as per the single-ion model [16,17]. However, as the 20% of the T_d A-site is occupied by Co^{2+} and Ni^2 ions, we can state that the present ferrite system can be considered as a normal ferrite. In case of pure phase of ZFO NPs, Zn ions occupy T_d A-site only whereas Fe ions occupied O_h-B site. Table 2 indicates that the percentage of individual phases of CNGaGdFO NPs and ZFO NPs does not varied for their different compositions. However, there is a marked change in the cation distribution for their mixed phase, which entirely depends upon their stoichiometry compositions.

3.2. Morphology

The surface analysis of H/S $(CNGaGdFO)_x/(ZFO)_y$ (x:y = 1:1, 1:2 and 2:1) NCs were proceeded by SEM, as seen in Fig. 2. The samples exhibited a cluster of small cubic particles with uniform distribution. It is obvious that the particles size varied with changing the fraction of each CNGaGdFO and ZFO NPs. The elemental analysis of H/S $(CNGaGdFO)_x/(ZFO)_y$ (x:y = 1:1, 1:2 and 2:1) NCs were achieved by using EDX and elemental mapping, as displayed in Figs. 3 and 4. It showed the elemental composition of NCs, such as Co, Ni, Ga, Gd, Fe, Zn and O with no trace of any impurities. The morphology and structure of H/S $(CNGaGdFO)_x/(ZFO)_y$ (x,y = 1:2) NCs were evaluated by TEM, HR-TEM and SAED (selected area electron diffraction) analyses, as seen in Fig. 5. These results support findings from SEM and XRD.

Table 1 – Refined structure parameters of CNGaGdFeO NPs, ZFO NPs and H/S $(CNGaGdFO)_x/(ZFO)_y$ (x:y = 1:1, 1:2, 1:3, 2:1, 3:1 and 4:1) NCs.

Product	D_{XRD} (nm)	a (Å)	V $(Å)^3$	χ^2 (chi^2)	R_{Bragg}
CNGaGdFeO NPs	47.9	8.3524	582.6850	12.7	5.3
$(CNGaGdFeO)_1/(ZFO)_1$ NCs	38.9	8.3619	584.6672	7.6	1.2
$(CNGaGdFeO)_1/(ZFO)_2$ NCs	48.4	8.3668	585.7145	9.0	1.3
$(CNGaGdFeO)_1/(ZFO)_3$ NCs	42.1	8.3734	587.0826	9.4	1.6
$(CNGaGdFeO)_2/(ZFO)_1$ NCs	59.1	8.3318	578.3906	15.8	2.2
$(CNGaGdFeO)_3/(ZFO)_1$ NCs	59.9	8.3337	578.7718	13.8	3.0
$(CNGaGdFeO)_4/(ZFO)_1$ NCs	52.4	8.3239	576.7385	14.0	4.1
ZFO NPs	50.4	8.4384	600.8633	7.5	1.4

3.3. Dielectric and electrical properties

Electrical and dielectric properties of H/S $(CNGaGdFO)_x/(ZFO)_y$ (x:y = 1:1, 1:2, 1:3, 2:1, 3:1 and 4:1) NCs were investigated in terms of AC conductivity as well as DC conductivity, activation energy, dielectric constant, dielectric loss in addition to the dissipation parameter. These factors were performed varying the applied frequency, the measured temperature and the various composition ratios of hard to soft spinel ferrites. Therefore, the dielectric properties of H/S $(CNGaGdFO)_x/(ZFO)_y$ (x:y = 1:1, 1:2, 1:3, 2:1, 3:1 and 4:1) NCs have been extensively studied including the referenced x and y spinel ferrites, of hard to soft spinel ferrites between 20 °C and 120 °C where frequency f ≤ 3.0 MHz.

3.3.1. Electrical parameter: AC conductivity

The AC (alternating current) conductivity can be utilized to study many behavior under the influence of the variable electric field such as charge mechanism, conduction mechanism and charge carrier performances. The AC conductivity for nearly all hard to soft spinel ferrites based on all given composition ratios, including reference spinel ferrites, is evaluated by the following equation:

$$\sigma_{ac}(\omega, T; r) = \omega\varepsilon_0\varepsilon'(\omega, T; r)tan\delta(\omega, T; r) \quad (1)$$

where ω: externally applied electric field's angular frequency, ε_0: absolute permittivity,ε': relative permittivity, r (=x/y): compositional rates of H/S spinel ferrites, T is the measured temperature, $tan\delta$: tangent loss. The three-dimensional representation of H/S $(CNGaGdFO)_x/(ZFO)_y$ (x:y = 1:1, 1:2, 1:3, 2:1, 3:1 and 4:1) NC AC conductivity measurements for a variety of compositional rates of hard to soft spinel ferrites including the hard and soft reference spinel ferrites is shown in Fig. 6. The conductivity at low frequencies has been found to depend on both the temperature and composition ratios of hard to soft spinel ferrites. In semi-logarithmic representation, conductivity increases linearly with temperature, while on the high frequency side it remains almost constant throughout temperature changes. As it can be seen from other spinel ferrites in the literature, it is obvious that the conductivities of both reference and compositional spinel ferrites obey power law rules with a variation of the exponent parameter and regional trends that vary depending on their composition ratio. It should be noted that conductivity variation with frequency is strongly dependent on the compositional rates of hard to soft spinel ferrites. For the r = x/y = 4:1 ratio, it starts to fluctuate with both frequency and temperature variables. It is also worth noting that the composition ratio of hard to soft spinel ferrites regulates conductivity as functions of temperature and frequency.

For all samples, it was observed that the conductivity fluctuated at the highest ratio of r = 4:1 with temperature, while it was more or less affected by frequency. It is therefore understood that the level of composition ratio greatly alters the spinel ferrite structures that cause the conduction mechanism. Except for the slight peak at r = 1:2 ratio, conductivity

Table 2 – Cation distribution of CNGaGdFeO NPs, ZFO NPs and H/S $(CNGaGdFO)_x/(ZFO)_y$ (x:y = 1:1, 1:2, 1:3, 2:1, 3:1 and 4:1) NCs.

Composition		T_d-A site	O_h-B site
ZFO NPs		$Zn_{1.0}$	$Fe_{2.0}$
CNGaGdFO NPs		$Co_{0.1}Ni_{0.1}Fe_{0.8}$	$Co_{0.4}Ni_{0.4}Ga_{0.01}Gd_{0.01}Fe_{1.18}$
1:1	NCs	$Zn_{0.5}Co_{0.05}Ni_{0.05}Fe_{0.4}$	$Co_{0.2}Ni_{0.2}Ga_{0.005}Gd_{0.005}Fe_{1.59}$
1:2	NCs	$Zn_{0.34}Fe_{0.66}$	$Co_{0.33}Ni_{0.33}Ga_{0.0066}Gd_{0.0066}Fe_{1.3268}$
1:3	NCs	$Zn_{0.25}Fe_{0.75}$	$Co_{0.375}Ni_{0.375}Ga_{0.0075}Gd_{0.0075}Fe_{1.235}$
2:1	NCs	$Zn_{0.66}Fe_{0.34}$	$Co_{0.17}Ni_{0.17}Ga_{0.0033}Gd_{0.0033}Fe_{1.6534}$
3:1	NCs	$Zn_{0.75}Fe_{0.25}$	$Co_{0.125}Ni_{0.125}Ga_{0.0025}Gd_{0.0025}Fe_{1.745}$
4:1	NCs	$Zn_{0.8}Fe_{0.2}$	$Co_{0.1}Ni_{0.1}Ga_{0.002}Gd_{0.002}Fe_{1.796}$

at high frequencies remains almost constant, while for all other samples it bends back diagonally from the high-temperature-low-frequency corner in the 3D plot, which maintains linearity trends in the semi-logarithmic plane. It has also been observed that the individual curve tendencies in conductivity of the reference spinel ferrites give rise to all the curve trends of the compositional hard to soft spinel ferrites.

3.3.2. *Electrical parameter: DC (direct current) conductivity and activation energy*

Arrhenius' plots of DC conductivity of H/S $(CNGaGdFO)_x/(ZFO)_y$ (x:y = 1:1, 1:2, 1:3, 2:1, 3:1 and 4:1) NCs for various composition ratios of hard to soft spinel ferrites, including hard and soft reference spinel ferrites, are shown in Fig. 7. As summarized in Table 3, it is clearly seen that the activation energy varies with the composition ratios of H/S $(CNGaGdFO)_x/(ZFO)_y$ (x:y = 1:1, 1:2, 1:3, 2:1, 3:1 and 4:1) NCs. For some reference and composite spinel ferrites, two regions above and below 400 meV in activation energy were observed according to composition ratios and high and low active temperature areas. The DC conductivity in soft spinel ferrite was found to be lower than that of both hard and composite spinel ferrites. In addition, it is obvious that DC conductivity increases with composition ratios regardless of the composite ratio of the r value, except for r = 1:3. The hard spinel ferrite seems to dominate the DC conductivity of composite spinel ferrites compared to the soft one. For r = x, 1:3 and 4:1 the activation energy presents two values independent upon a variety of contributions to thermal energy while a weak contribution takes place for r = 4:1. The activation energy for r = y, 1:1, 1:2, 2:1 and 3:1 has a single value of about 400 meV, but it should be noted that soft spinel ferrite shows the single lowest value of activation energy, while that of hard spinel ferrite has the highest value of about 761 meV. Consequently, for each of the hard and soft spinel ferrite as a reference and the composite spinel ferrites based on composite rates, DC conductivity can be expressed as follows:

$$\sigma_{dc}(T,r) = \sigma_0(r)\exp\left(-\frac{E_a(r)}{k_B T}\right) \quad (2)$$

where σ_0: conductivity at absolute temperature for a certain composition ratio of hard to soft spinel ferrites, k_B: Boltzmann constant, E_a: activation energy, r: composition ratio. The E_a is affected by the relaxation temperature, which can be correlated with the composition ratio. Such a tendency is crucial in the conduction mechanism of both referenced spinel ferrites and all composite spinel ferrites. Therefore, Verwey mechanism can be used to interpret the conduction mechanism in all spinel ferrites in this study comprehensively [18].

The composition ratio induces structural effects which lead to the replacement of electrons/holes among similar ion types or single exchange of Fe (III) and Fe (II) ions in multiple

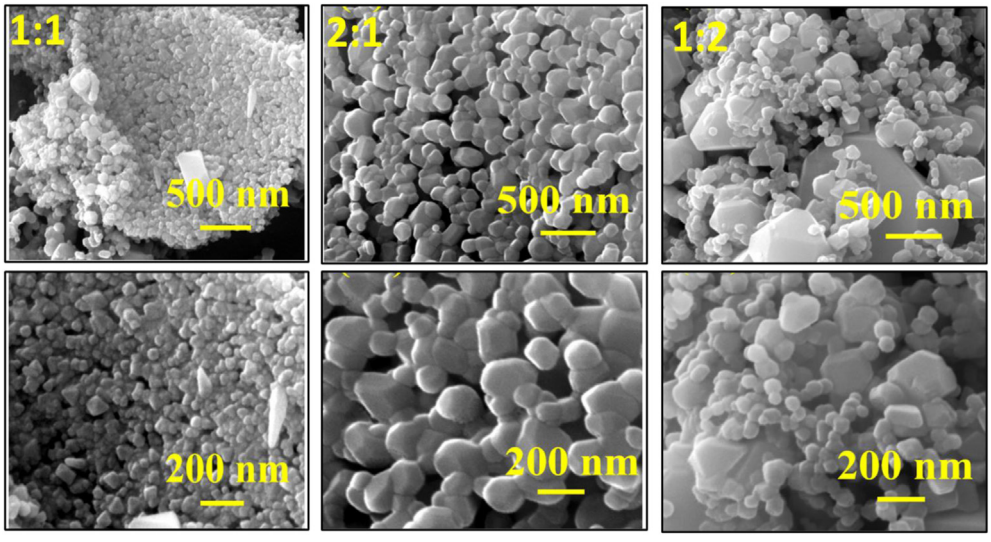

Fig. 2 – SEM images of H/S $(CNGaGdFO)_x/(ZFO)_y$ (x:y = 1:1, 1:2, 2:1) NCs.

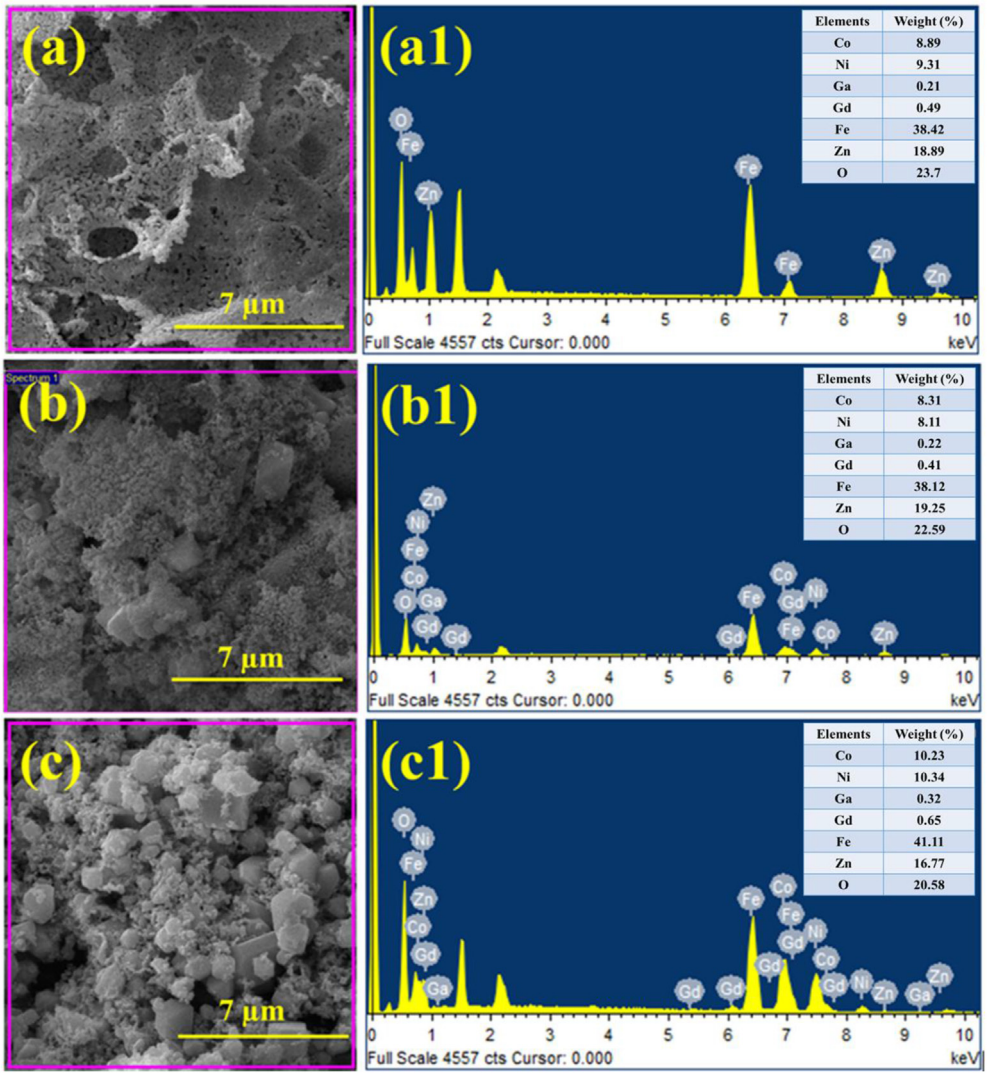

Fig. 3 – SEM micrographs and EDX spectra of $(CNGaGdFO)_x/(ZFO)_y$ a) x:y = 1:1, b) x,y = 1:2 and c) x,y = 2:1 NCs.

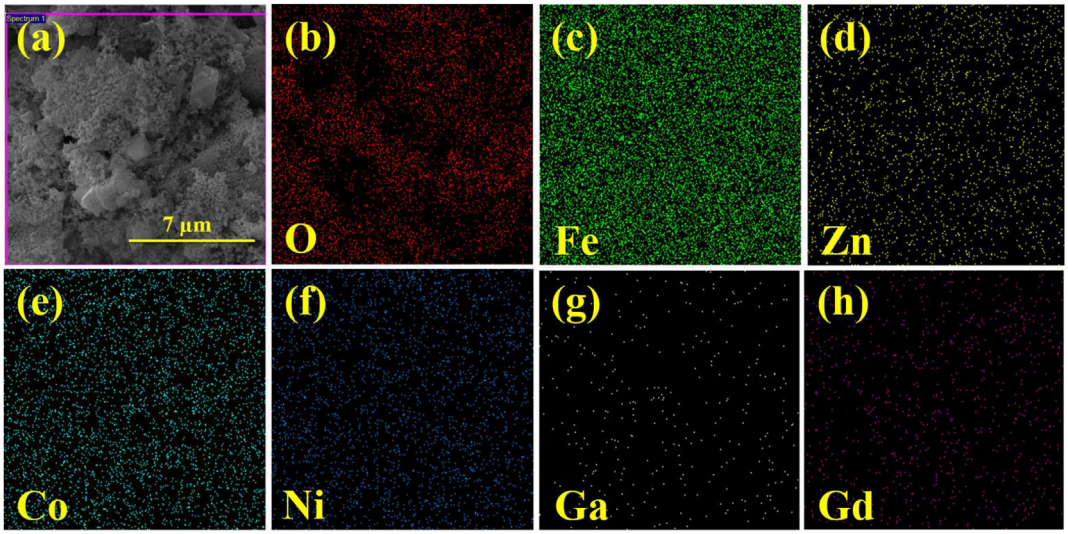

Fig. 4 – The elemental mappings of H/S $(CNGaGdFO)_x/(ZFO)_y$ (x,y = 1:2) NCs.

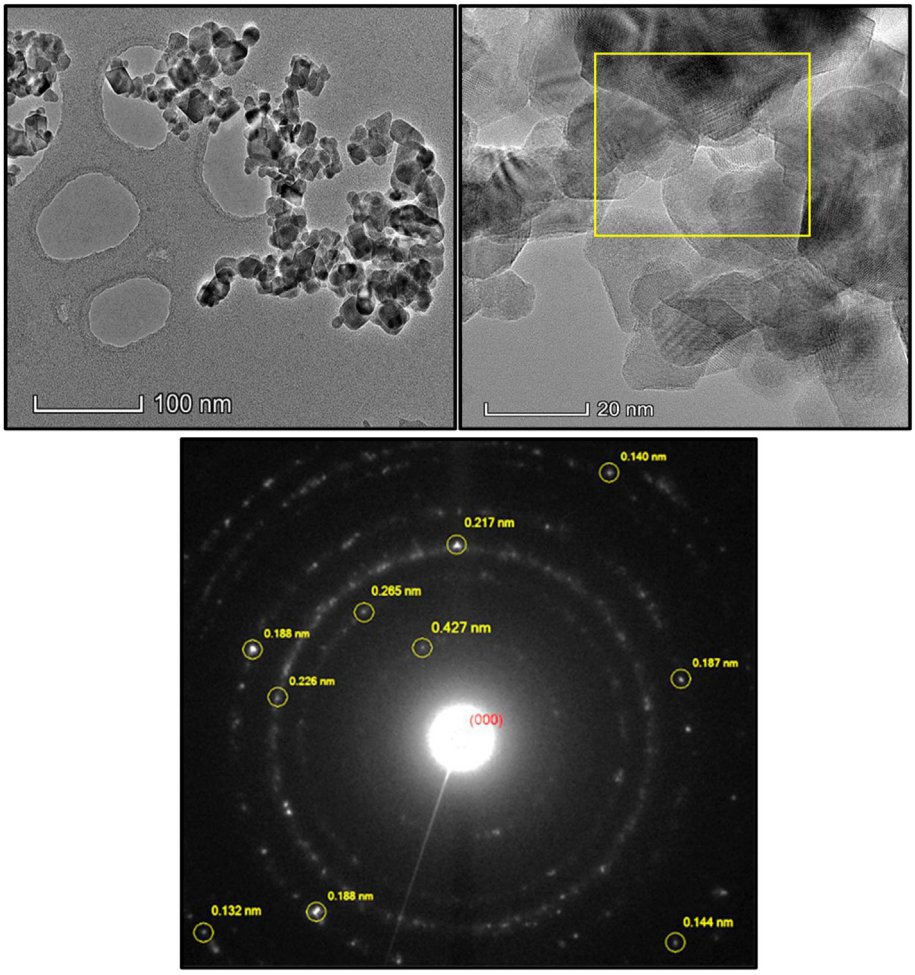

Fig. 5 – TEM, HR-TEM micrographs and SAED pattern of H/S $(CNGaGdFO)_x/(ZFO)_y$ (x,y = 1:2) NCs.

valence states which results as the conduction. Slightly more contribution to the conduction mechanism could also come from the polaron/electron hopping process [19]. Thus, a variation in the composition ratio also has an influence on the charged carriers drift mobility in spinel ferrites. A rise in the temperature indicates the rise of E_a resulting from the thermal energy of charge carriers in spinel ferrite samples. Therefore, considering the ion distribution structural effect in both reference and composite spinel ferrites, a reasonable elucidation can be deduced for this conduction mechanism [20].

3.3.3. *Dielectric parameter: dielectric constant*

The dielectric constant (ε_r) of CoNiGaGdFeO-$ZnFe_2O_4$ H/S NCs for various composite ratios, including reference hard and soft spinel ferrites, was characterized in the 3D graphs in Fig. 8 for temperatures ranging from 20 °C to 120 °C and frequency $f \leq 3.0$ MHz. As seen from the figure, the ε_r drops as the frequency (f) increases, roughly like hard spinel ferrite. Both soft spinel ferrite and spinel ferrite with a 4:1 composite ratio showed a completely different behaviour. However, other composite rational spinel ferrites exhibited similar behaviour. It is also obvious that the composite ratio and temperature have some effect on ε_r. It should also be noted that composite spinel ferrite with soft spinel ferrite and high hard spinel ferrite ratio shows us a very different behaviour and therefore it will not be easy to understand this behaviour at the moment. Perhaps an excessive amount of hard spinel ferrite may cause a structural transition of the dielectric property of the composite structure. For spinel ferrite with 4:1 composite ratio, it can be observed that the dielectric constant fluctuates against both frequency and temperature changes at low and medium frequency values. On the other hand, in soft spinel ferrite it is known from the graph that the dielectric constant shows a completely different trend. That is, it is seen that the dependence of ε_r to the temperature is extremely high, especially in the smaller and medium frequency region. It can be stated in general that the dielectric constant follows the power exponent law $\varepsilon'(\omega)\alpha\omega^n$.

The variation of the ε_r as a function of frequency was found to be very complex for both 4:1 compound ratios and hard and

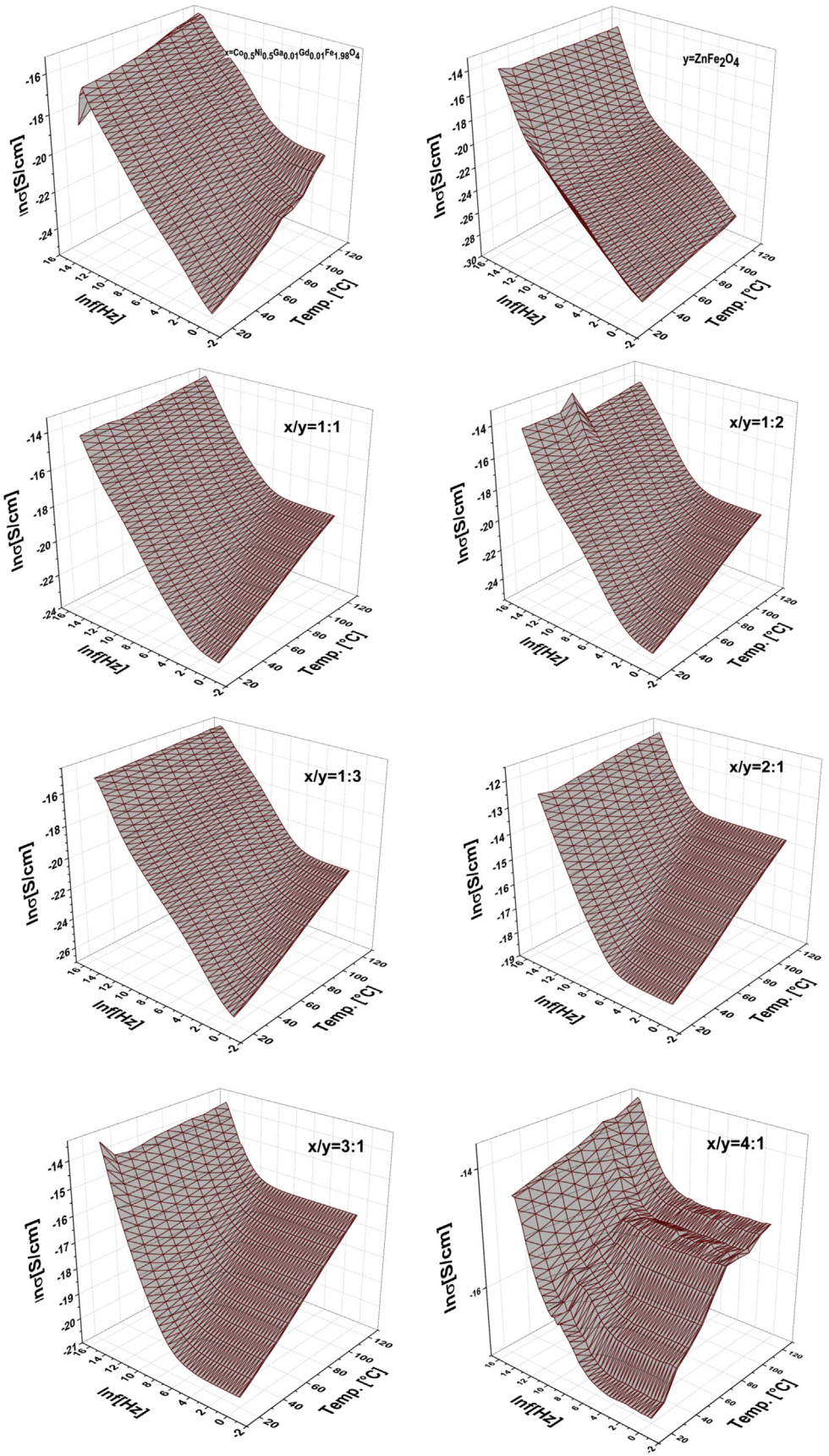

Fig. 6 – AC conductivities of x = $Co_{0.5}Ni_{0.5}Ga_{0.01}Gd_{0.01}Fe_{1.98}O_4$, y = $ZnFe_2O_4$ NPs and H/S $(CNGaGdFO)_x/(ZFO)_y$ (x:y = 1:1, 1:2, 1:3, 2:1, 3:1 and 4:1) NCs.

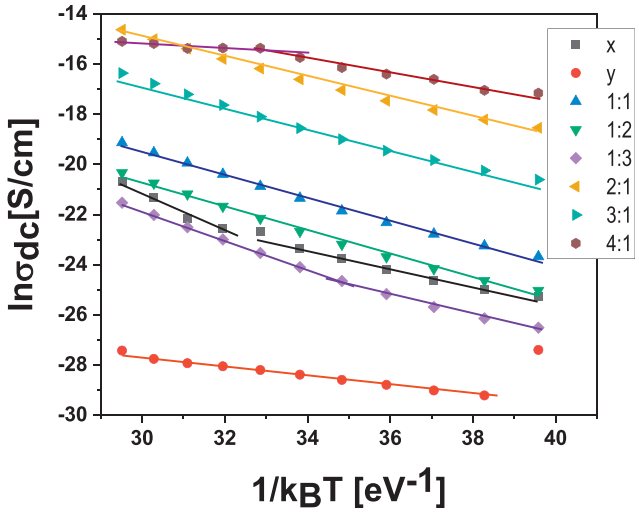

Fig. 7 – Arrhenius plots of DC conductivities of $x = Co_{0.5}Ni_{0.5}Ga_{0.01}Gd_{0.01}Fe_{1.98}O_4$, $y = ZnFe_2O_4$ NPs and H/S $(CNGaGdFO)_x/(ZFO)_y$ (x:y = 1:1, 1:2, 1:3, 2:1, 3:1 and 4:1) NCs.

soft spinel ferrites. However, the variation in dielectric constant for other compositional spinel ferrites with a different ratio is somewhat regulated. Hence, the dielectric properties of CoNiGaGdFeO-$ZnFe_2O_4$ H/S NCs are distributed at smaller frequency values which is originating from a space charge polarization.

When the two-layer model [21] is carefully considered, we can deduce that highly conductive grains found at grain boundaries which act as insulators can be correlated with space charge polarization. Thus, grains are less dominant than grain boundaries at smaller frequency values. Although the dielectric constant is directly related to the change in grain boundaries, it can sometimes be less frequency dependent at higher frequencies. As it can be seen from all the graphs in Fig. 8, it can be noted that the exchange charge carriers between ferrous and ferric ions in the octahedral regions can follow the alteration in the electric field straightforwardly, unless it exceeds a particular value depending on x:y ratio. The frequency-dependent decrease of the dielectric constant denotes the electronic substitution between ferrous and ferric ions, that offers electrical polarization affinities in H/S $(Co_{0.5}Ni_{0.5}Ga_{0.01}Gd_{0.01}Fe_{1.98}O_4)_x/(ZnFe_2O_4)_y$ (x:y = 1:1, 1:2, 1:3,2:1,3:1 and 4:1) NCs. As a result, when various compositional spinel ferrites are studied, it can be easily understood how numerous aspects such as cation distribution, structural change, charge polarization and density triggered by composition ratios affect their dielectric and electrical behaviour. Consequently, the dielectric parameters varying with the frequency can be credited to the conduction mechanism in the majority of composition ratios of hard to soft spinel ferrites, which can be explained by a phenomenological method with Koop's model [21].

3.3.4. *Dielectric parameter: dielectric loss*

The dielectric loss plots of CoNiGaGdFeO-$ZnFe_2O_4$ hard to soft spinel ferrite N/Cs for various x:y values is represented in Fig. 9. The dielectric loss shows a sharp decline with increasing frequency throughout the temperature range except the soft spinel ferrite. The dielectric loss rises slightly as the temperature rises for the spinel ferrite and compositional of spinel ferrites, while it decreases first and then increase with values along both the frequency and temperature for soft spinel ferrite. For the composition ratio r = 4:1 of hard to soft spinel ferrite, the dielectric loss exactly matches the power law exponent compared to other compositional spinel ferrites, which gives us a chance to change the loss parameter with a composition ratio. It is seen that the 3-dimensional curve of dielectric loss, dependent on frequency and temperature, in such a curve is similar to the shape of a recliner chair. It was observed that the change decreased rapidly with frequency, generally depending on x:y ratio, then the valley region was formed and then decreased again. While the temperature dependence was recorded for all spinel ferrites, it was found to be almost independent for spinel ferrite with r = 4:1. At low frequencies, it shows distinct, but different rises as the temperature rises, varying with x:y ratio. The temperature dependence at lower frequencies also decreased with increasing composition ratio, such as r = 4:1.

3.3.5. *Dissipation parameter: tangential loss*

Tangential loss (*tanδ*) refers to the quantitative dispersion of electrical energy resulting from some different physical concepts such as electrical conduction, dielectric relaxation, dielectric resonance and attenuation from nonlinear processes. Therefore, dissipation parameters of H/S $(Co_{0.5}Ni_{0.5}Ga_{0.01}Gd_{0.01}Fe_{1.98}O_4)_x/(ZnFe_2O_4)_y$ (x:y = 1:1, 1:2, 1:3,2:1,3:1 and 4:1) NCs are shown in Fig. 10 for various compositional ratios including the referenced hard and soft spinel ferrites and analysed as a 3D representation function of temperatures from 20 °C to 120 °C with f ≤ 3.0 MHz. The *tanδ* was observed to decrease sharply with increasing frequency at all temperature values. It is worth mentioning that similarities between ε_r and *tanδ* as well as the dissipation parameters of most compositional spinel ferrites are remarkably high, but that soft spinel ferrite and 4:1 compositional spinel ferrite show much more inconsistency than other spinel ferrites. It is inferred that all dielectric parameter trends usually vary with diverse parameters such as frequency, temperature and composition ratios. As a result, the *tanδ* of H/S $(Co_{0.5}Ni_{0.5}Ga_{0.01}Gd_{0.01}Fe_{1.98}O_4)_x/$

Table 3 – Activation energies of $x = Co_{0.5}Ni_{0.5}Ga_{0.01}Gd_{0.01}Fe_{1.98}O_4$, $y = ZnFe_2O_4$ NPs and H/S $(CNGaGdFO)_x/(ZFO)_y$ (x:y = 1:1, 1:2, 1:3, 2:1, 3:1 and 4:1) NCs.

x:y	x		y	1:1	1:2	1:3		2:1	3:1	4:1	
T Region	T_{high}	T_{low}	T_{all}	T_{all}	T_{all}	T_{high}	T_{low}	T_{all}	T_{all}	T_{high}	T_{low}
E_g (meV)	761	350	171	452	466	587	390	399	423	110	301

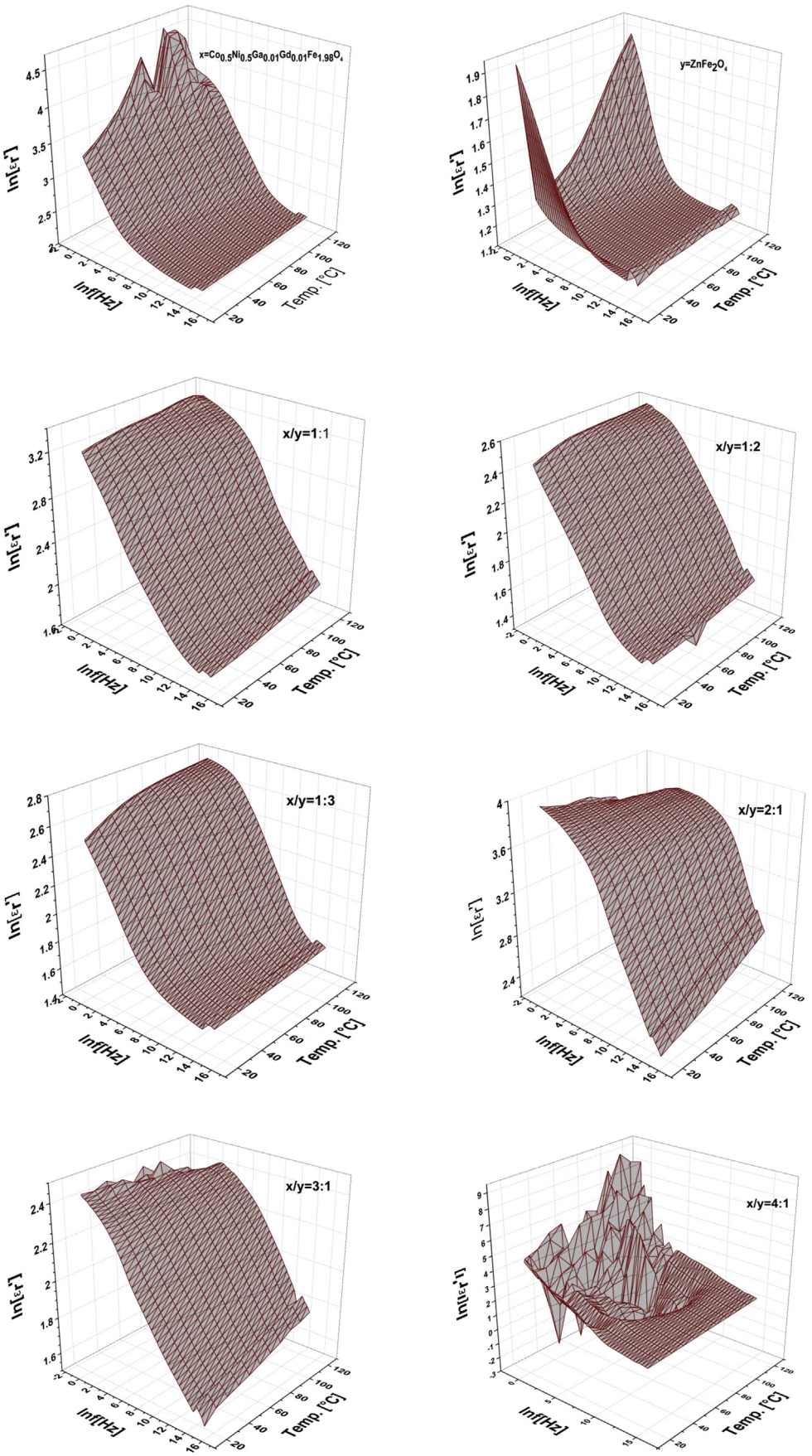

Fig. 8 – Dielectric constant of x = $Co_{0.5}Ni_{0.5}Ga_{0.01}Gd_{0.01}Fe_{1.98}O_4$, y = $ZnFe_2O_4$ NPs and H/S $(Co_{0.5}Ni_{0.5}Ga_{0.01}Gd_{0.01}Fe_{1.98}O_4)_x/(ZnFe_2O_4)_y$ (x:y = 1:1, 1:2, 1:3,2:1,3:1 and 4:1) NCs.

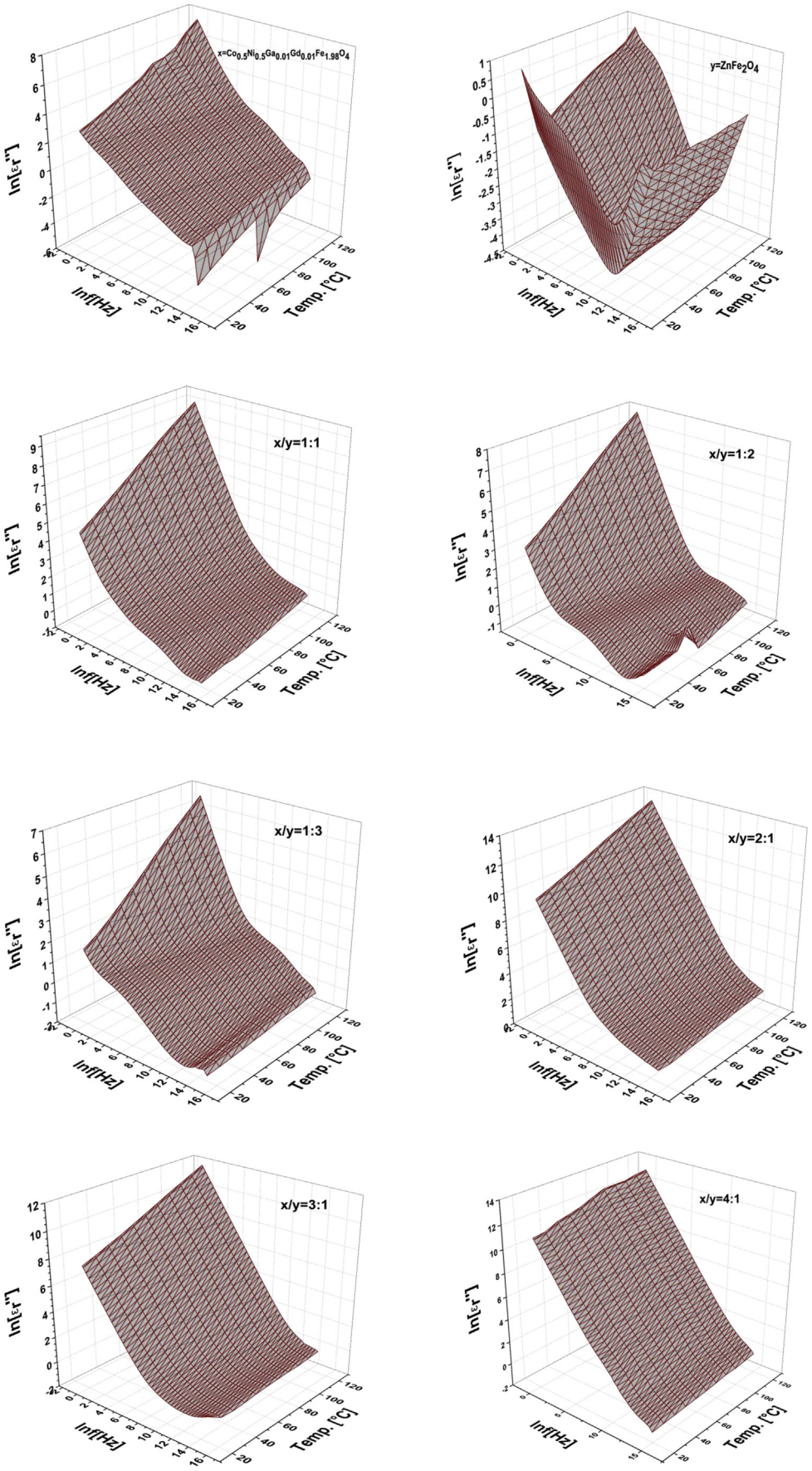

Fig. 9 – Dielectric loss of x = $Co_{0.5}Ni_{0.5}Ga_{0.01}Gd_{0.01}Fe_{1.98}O_4$, y = $ZnFe_2O_4$ NPs and the ratios of the H/S $(Co_{0.5}Ni_{0.5}Ga_{0.01}Gd_{0.01}Fe_{1.98}O_4)_x/(ZnFe_2O_4)_y$ (x:y = 1:1, 1:2, 1:3,2:1,3:1 and 4:1) NCs.

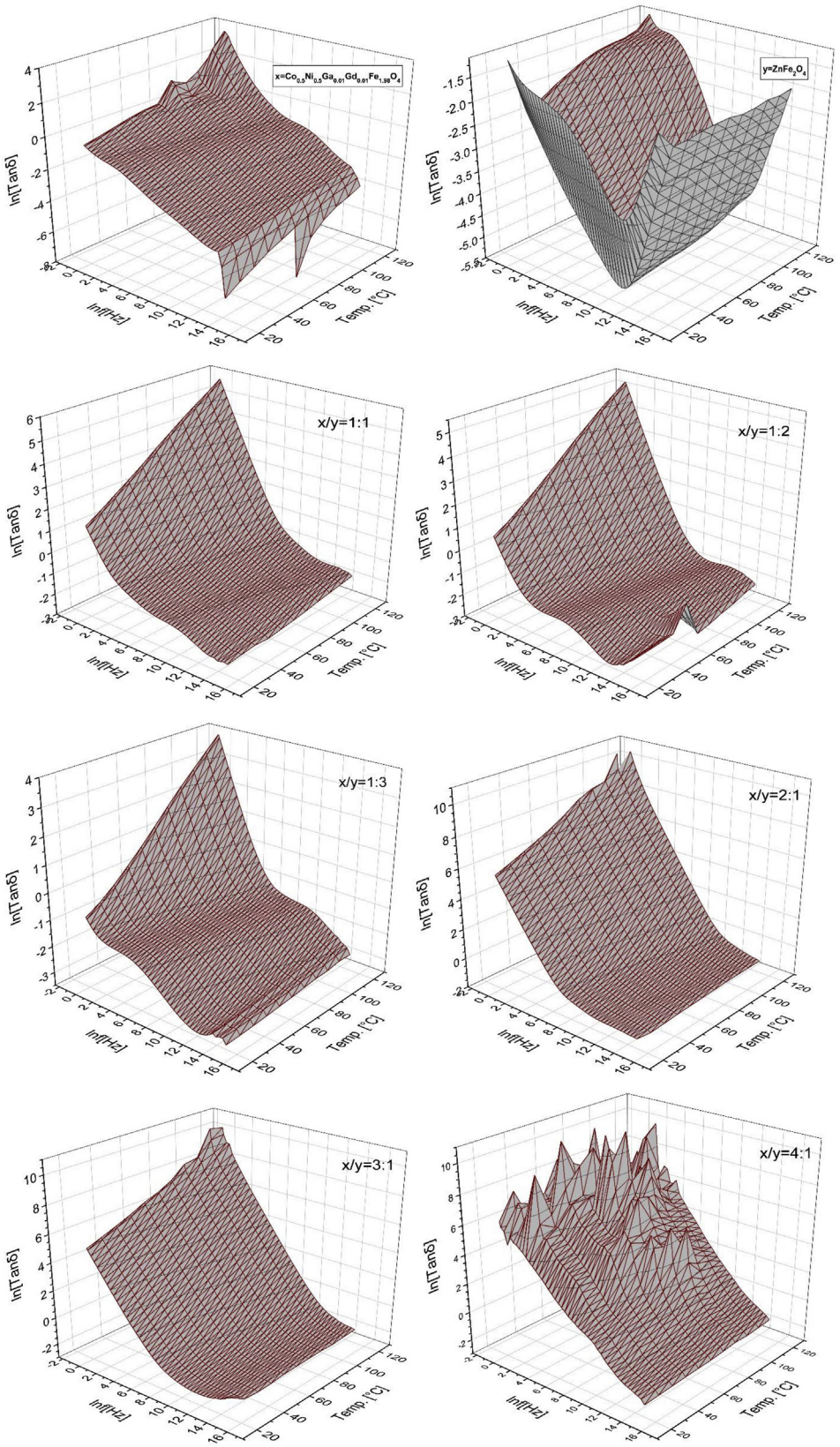

Fig. 10 – Tangential loss of x = $Co_{0.5}Ni_{0.5}Ga_{0.01}Gd_{0.01}Fe_{1.98}O_4$, y = $ZnFe_2O_4$ NPs and the ratios of the H/S $(Co_{0.5}Ni_{0.5}Ga_{0.01}Gd_{0.01}Fe_{1.98}O_4)_x/(ZnFe_2O_4)_y$ (x:y = 1:1, 1:2, 1:3,2:1,3:1 and 4:1) NCs.

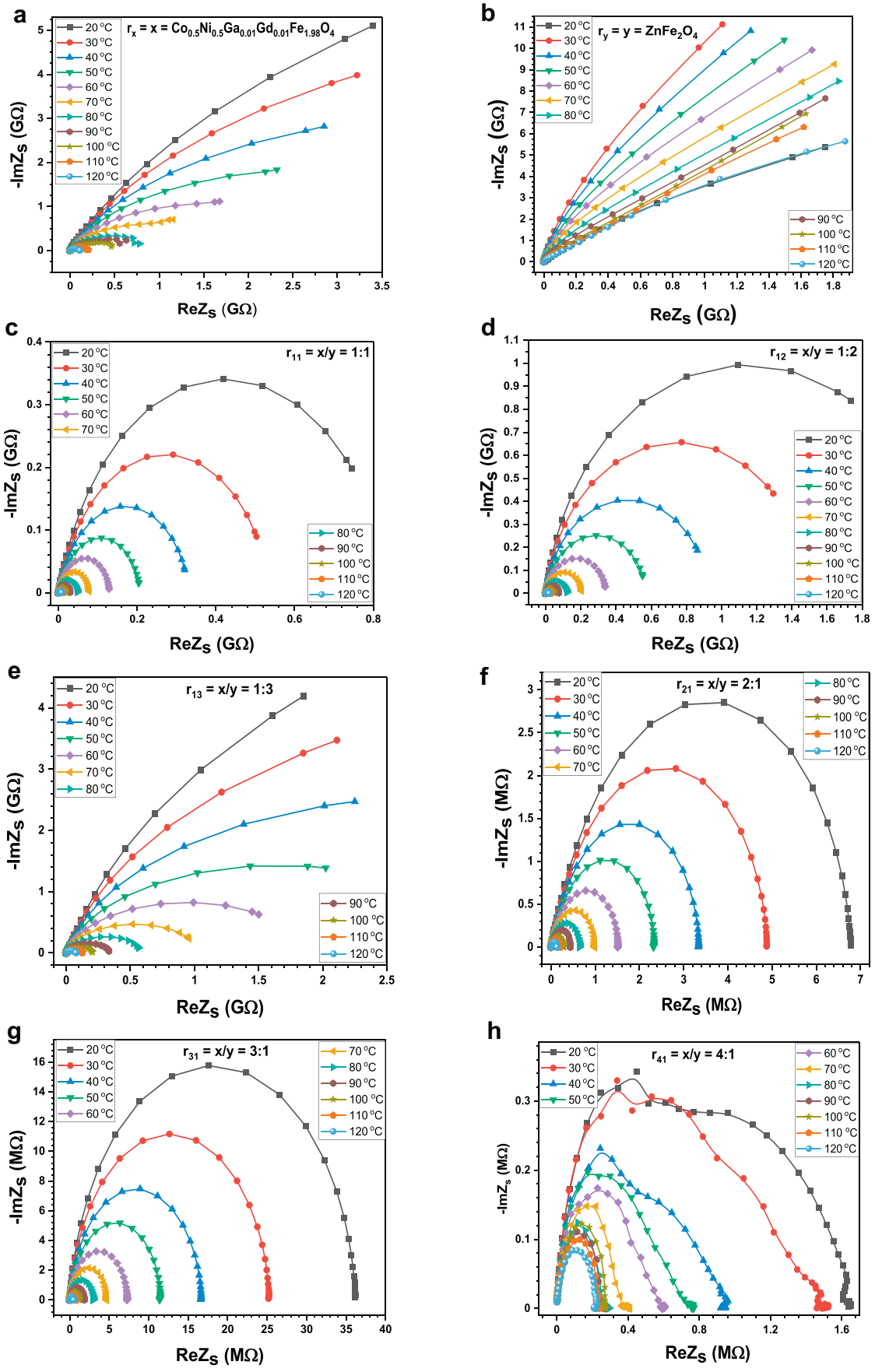

Fig. 11 – Impedance spectra of Cole–Cole plots (-ImZ$_s$ versus ReZ$_s$) of (a) r_x = x = $Co_{0.5}Ni_{0.5}Ga_{0.01}Gd_{0.01}Fe_{1.98}O_4$ NPs as hard ferrite, (b) r_y = y = $ZnFe_2O_4$ NPs as soft ferrite, and compositional hard to soft ferrites as (c) r_{11} = x:y = 1:1, (d) r_{12} = x:y = 1:2, (e) r_{13} = x:y = 1:3, (f) r_{21} = x:y = 2:1, (g) r_{31} = x:y = 3:1 and (h) r_{41} = x:y = 4:1. Applied frequency varies from 3.0 MHz down to 1.0 Hz along the semicircles.

$(ZnFe_2O_4)_y$ (x:y = 1:1, 1:2, 1:3,2:1,3:1 and 4:1) NCs is highly dependent on both temperature and frequency, which is quite important for numerous dielectric and electrical parameters in several technological applications as well as biomedicine, including various biosensors, gas sensors and MRI contrast agents [19,22].

3.3.6. *Cole–Cole plotting*

The frequency dependent dielectric parameter of any ferrite compound can be explained with complex permittivity (ε*), complex impedance (Z*) and dielectric loss or dissipation factor (tan(δ)). So, the correlation between real parts (ε′, Z′) and imaginary (ε″, Z″) parts of complex parameters is: $\varepsilon^* = \varepsilon' + i\varepsilon''$; $Z^* = Z' + iZ'' = (1/iC_0\varepsilon^*\omega)$; $\tan(\delta) = \varepsilon''/\varepsilon' = Z'/Z''$, where C_0: free geometrical capacitance. Such equations propose a widespread range of exploration possibilities for numerous parameter having graphical analysis under different frequency and temperature values. A functional separation of grain and grain boundary phenomena probably depends on the selection of an equivalent circuit appropriate to represent compositional properties. From the microstructural point of view, it can be seen that the hard ferrite and various compositional ferrites were constituted from grain boundaries and grains which carry out various conductivity and dielectric permittivity [23,24]. The grain boundary and grain existence involvement and influence of electrode interfaces can be clearly interpreted by the Cole–Cole impedance plot. Z′ and Z″ parts of the complex impedance can be expressed as [25]:

$$Z'(\omega) = \frac{R_g}{1+(\omega R_g C_g)^2} + \frac{R_{gb}}{1+(\omega R_{gb} C_{gb})^2} + \frac{R_{el}}{1+(\omega R_{el} C_{el})^2} \quad (3)$$

$$Z''(\omega) = R_g\left[\frac{\omega R_g C_g}{1+(\omega R_g C_g)^2}\right] + R_{gb}\left[\frac{\omega R_{gb} C_{gb}}{1+(\omega R_{gb} C_{gb})^2}\right] + R_{el}\left[\frac{\omega R_{el} C_{el}}{1+(\omega R_{el} C_{el})^2}\right] \quad (4)$$

where R_g, C_g, R_{gb}, C_{gb} and C_{el} R_{el} are resistance and capacitance of grain, the grain boundary and electrode interfaces, respectively, ω is the angular frequency. The Cole–Cole graphical representation shows that the effect of the electrode interface on surface charge polarizations is related to high temperatures and is highly effective for grain and grain boundary contribution at its high values [26].

To understand the relaxation mechanism of various compositional ferrites, a well-known Cole–Cole graph is used to explain what kind of dielectric relaxation is present in the frequency-dependent response of various compositional ferrites. The complex impedance Cole–Cole plot is represented to investigate the electric transport mechanism in various compositional hard-to-soft ferrites. The impedance spectra of Cole–Cole plots (-ImZ_s versus ReZ_s) of (a) r_x = x = $Co_{0.5}Ni_{0.5}Ga_{0.01}Gd_{0.01}Fe_{1.98}O_4$ NPs as hard ferrite, (b) r_y = y = $ZnFe_2O_4$ NPs as soft ferrite, and compositional hard to soft ferrites as (c) r_{11} = x:y = 1:1, (d) r_{12} = x:y = 1:2, (e) r_{13} = x:y = 1:3, (f) r_{21} = x:y = 2:1, (g) r_{31} = x:y = 3:1 and (h) r_{41} = x:y = 4:1 are shown in Fig. 11. Applied frequency varies from 3.0 MHz down to 1.0 Hz along the semicircles towards to the origin of the curves. As the temperature increases, the diameter of the semicircles of the Cole–Cole plots narrows. It is observed that hard ferrite is dominant in the formation of the semicircles, and the semicircles are deteriorated at the excess composition ratio such as r_{41} = 4:1. Also, soft ferrite appears to be more dominant in compositional ferrites with the smallest r_{13} = 1:3 ratio. It was also measured that the real part of the complex impedance for hard ferrite is higher than that of soft ferrite, while the imaginary part is higher for soft ferrite. This type of interpretation represents the fact that the system is non-Debye-type systems, and the trends is known to result from ionic hopping conduction between ferric and ferrous ions with a wide relaxation time distribution [27,28]. The single semicircle observed for almost all compositional ferrites indicates some type of relaxation at temperatures up to 120 °C. The diameter of the semicircles decreases with increasing temperature, suggesting a temperature dependent mechanism of relaxation. It is also noted that at higher temperatures more electrons are thermally excited, thus further shortening the relaxation time of the carrier. Therefore, the dispersed thermal energy helps the formed dipoles to follow the motion of the externally applied alternative electric field. This characteristic mechanism describes the existence of temperature-dependent electrical relaxation events in compositional ferrites [29,30].

4. Conclusion

The H/S $(CNGaGdFO)_x/(ZFO)_y$ (x:y = 1:1, 1:2, 1:3, 2:1, 3:1 and 4:1) NCs have been synthesized in pot sol–gel auto combustion approach. The XRD and EDX analyses proved the purity of all products (including NPs and NCs). The cubic morphology of all products has been verified by TEM and TEM techniques. It is obvious that H/S $(Co_{0.5}Ni_{0.5}Ga_{0.01}Gd_{0.01}Fe_{1.98}O_4)_x/(ZnFe_2O_4)_y$ (x:y = 1:1, 1:2, 1:3, 2:1, 3:1 and 4:1) NCs have a remarkable effect on electrical and dielectric properties. AC conductivity is clearly strongly dependent on frequency, temperature and composition ratios. It can be said that conductivity generally obeys the power law rule of frequency. For all composition ratios, including hard and soft spinel ferrites, the dc conductivity decreases with an increase in the thermal energy of the $(k_BT)^{-1}$ parameter. The activation energy varies with changes in composition ratios, some of which have transition temperatures of about 60–80 °C, such as hard spinel ferrite and compositional spinel ferrites with r = 1:3 and r = 4:1. The dielectric constant shows the well-known dielectric distribution with frequency under various composition ratios of hard to soft spinel ferrites. It has been noted that both the dielectric constant and dielectric loss of compositional spinel ferrites decrease with increasing frequency, which is generally observed in normal behaviour for most spinel ferrites. It has been observed that the compositional ferrites show dielectric relaxation, which is found to be of the non-Debye type, and the relaxation frequency shifts to the higher side with increasing temperature. Therefore, such trends in electrical and dielectric parameters based on composition ratios open up many possibilities for certain technological applications such as various types of sensors, contrast agents used for MRI devices and magnetic hyperthermia.

Declaration of Competing Interest

The authors declare that they have no known competing financial interests or personal relationships that could have appeared to influence the work reported in this paper.

REFERENCES

[1] Kefeni KK, Mamba BB. Photocatalytic application of spinel ferrite nanoparticles and nanocomposites in wastewater treatment. Review/Sustainable Materials and Technologies 2020;23:e00140.

[2] Algaroua NA, Slimani Y, Almessiere MA, Rehman S, Younas M, Unal B, et al. Developing the magnetic, dielectric and anticandidal characteristics of $SrFe_{12}O_{19}/(Mg_{0.5}Cd_{0.5}Dy_{0.03}Fe_{1.97}O_4)_x$ hard/soft ferrite nanocomposites. J. Taiwan Inst. Chem. Eng. 2020;113:344–62.

[3] Almessiere MA, Slimani Y, Trukhanov AV, Sadaqat A, Demir Korkmaz A, Algarou NA, et al. Review on functional bi-component nanocomposites based on hard/soft ferrites: structural, magnetic, electrical and microwave absorption properties. Nano-Structures & Nano-Objects 2021;26:100728.

[4] Feng C, Liu X, Or SW, Ho SL. Exchange coupling and microwave absorption in core/shell-structured hard/soft ferrite-based $CoFe_2O_4/NiFe_2O_4$ nanocapsules. AIP Adv 2017;7:056403.

[5] Houshiar M, Zebhi F, Razi ZJ, Alidoust A, Askari Z. Synthesis of cobalt ferrite ($CoFe_2O_4$) nanoparticles using combustion, coprecipitation, and precipitation methods: a comparison study of size, structural, and magnetic properties. J Magn Magn Mater 2014;371:43–8.

[6] Hoque SM, Hossain Md S, Choudhury S, Akhter S, Hyder F. Synthesis and characterization of $ZnFe_2O_4$ nanoparticles and its biomedical applications. Mater Lett 2016;162:60–3.

[7] Mahalakshmi S, Srinivasa Manja K, Nithiyanantham S. Electrical properties of nanophase ferrites doped with rare earth ions. J Supercond Nov Magnetism 2014;27:2083–8.

[8] Almessiere MA, Ünal B, Slimani Y, Demir Korkmaz A, Baykal A, Ercan I. Electrical properties of La^{3+} and Y^{3+} ions substituted $Ni_{0.3}Cu_{0.3}Zn_{0.4}Fe_2O_4$ nanospinel ferrites. Results in Physics 2019;15:1027552.

[9] M.A. Almessiere, Y.A. Slimani, M. Hassan, M.A. Gondal, E. Cevik, A. Baykal, Investigation of hard/soft $CoFe_2O_4/NiSc_{0.03}Fe_{1.97}O_4$ nanocomposite for energy storage applications, DOI: 10.1002/er.6916.

[10] Pilati V, Gomes RC, Gomide G, Coppola P, Silva FG, Paula FLO, et al. Core/shell nanoparticles of non-stoichiometric Zn–Mn and Zn–Co ferrites as thermosensitive heat sources for magnetic fluid hyperthermia. J Phys Chem C 2018;122:3028–38.

[11] Nikolic AS, Boskovic M, Spasojevic V, Jancar B, Antic B. Magnetite/Mn-ferrite nanocomposite with improved magnetic properties. Mater Lett 2014;120:86–9.

[12] Mansour SF, Imam NG, Goda S, Abdo MA. Constructive coupling between $BiFeO_3$ and $CoFe_2O_4$; promising magnetic and dielectric properties. J. Mater. Res.Techn. 2020;9:1434–46.

[13] Mohammadabadi FH, Masoudpanah SM, Alamolhoda S, Koohdar HR. Electromagnetic microwave absorption properties of high entropy spinel ferrite $((MnNiCuZn)_{1-x}Co_xFe_2O_4)$/graphene nanocomposites. J. Mater. Res.Techn. 2021;14:1099–111.

[14] Shirsath SE, Mane ML, Yasukawa Y, Liu X, Morisako A. Chemical tuning of structure formation and combustion process in $CoDy_{0.1}Fe_{1.9}O_4$ nanoparticles: influence@pH. J Nano Res 2013;15:1976.

[15] Shirsath SE, Mane ML, Yasukawa Y, Liu X, Morisakoa A. Self-ignited high temperature synthesis and enhanced super-exchange interactions of Ho^{3+}–Mn^{2+}–Fe^{3+}–O^{2-} ferromagnetic nanoparticles. Phys Chem Chem Phys 2014;16:2347–57.

[16] Shirsath SE, Wang D, Jadhav SS, Mane ML, Li S. Ferrites obtained by sol-gel method. In: Klein L, Aparicio M, Jitianu A, editors. Handbook of sol-gel science and technology. Cham: Springer; 2018. p. 695–735.

[17] Shirsath SE, Liu X, Yasukawa Y, Li S, Morisako A. Switching of magnetic easy-axis using crystal orientation for large perpendicular coercivity in $CoFe_2O_4$ thin film. Sci Rep 2016;6:30074.

[18] Piekarz P, Parlinski K, Oleś Aj M. Mechanism of the Verwey transition in magnetite. Phys Rev Lett 2006;97:156402.

[19] Almessiere MA, Unal B, Auwal AI, Slimani Y, Aydin H, Manikandan A, et al. Impact of calcination temperature on electrical and dielectric properties of $SrGa_{0.02}Fe_{11.98}O_{19}$-$Zn_{0.5}Ni_{0.5}Fe_2O_4$ hard/soft nanocomposites. J Mater Sci Mater Electron 2021;32:16589–600.

[20] Alahmari F, Almessiere MA, Ünal B, Slimani Y, Baykal A. Electrical and optical properties of $Ni_{0.5}Co_{0.5-x}Cd_xNd_{0.02}Fe_{1.78}O_4$ ($x \leq 0.25$) spinel ferrite nanofibers. Ceram Int 2020;46:24605–14.

[21] Koops CG. On the dispersion of resistivity and dielectric constant of some semiconductors at audio frequencies. Phys Rev 1951;83:121–4.

[22] Slimani Y, Unal B, Almessiere MA, Demir-Korkmaz A, Shirsath SE, Yasine G, et al. Investigation of structural and physical properties of Eu^{3+} ions substituted $Ni_{0.4}Cu_{0.2}Zn_{0.4}Fe_2O_4$ spinel ferrite nanoparticles prepared via sonochemical approach. Results Phys 2020;17:10306.

[23] Dygas JR, Fafilek G, Breiter MW. Study of grain boundary polarization by two-probe and four-probe impedance spectroscopy. Solid State Ionics 1999;119:115–25.

[24] Rekaby M. Dielectric response and Cole–Cole plot analysis for $(Zn_{0.91}Mn_{0.03}Co_{0.06}O)_x/Cu_{0.5}Tl_{0.5}Ba_2Ca_2Cu_3O_{10-\delta}$ diluted magnetic semiconductor/superconductor composites. Appl Phys A 2020;126:664–73.

[25] Langhammer HT, Makovec D, Pu Y, Abicht H-P, Drofenik M. Grain boundary reoxidation of donordoped barium titanate ceramics. J Eur Ceram Soc 2006;26:2899–907.

[26] Karmakar S, Behera D. High-temperature impedance and alternating current conduction mechanism of $Ni_{0.5}Zn_{0.5}WO_4$ micro-crystal for electrical energy storage application. J Australas Ceram Soc 2020;56:1253–9.

[27] Song CH, Kim M, Lee SM, Choi HW, Yang YS. Impedance analysis and low-frequency dispersion behavior of $Bi_4Ti_3O_{12}$ glass. J Kor Phys Soc 2010;56:462–6.

[28] Chaouchi A, Kennour S. Impedance spectroscopy studies on lead free $(Ba_{0.85}Ca_{0.15})(Ti_{0.9}Zr_{0.1})O_3$ Ceramics, Process. Appl Ceram 2012;6:201–7.

[29] Yahia IS, Fadel M, Sakr GB, Shenouda SS, Yakuphanoglu F, Farooq WA. Impedance spectroscopy of nanostructure *p*-$ZnGa_2Se_4$/*n*-Si heterojunction diode. Acta Phys Pol, A 2011;120:563–6.

[30] Bakkali H, Dominguez M, Batlle X, Labarta A. Equivalent circuit modeling of the ac response of Pd-ZrO_2 granular metal thin films using impedance spectroscopy. J Phys D: Appl Phys 2015;48:335306.